

Efficient shrub modelling based on terrestrial laser scanning (TLS) point clouds

Minglei Li, Zheng Li, Meng Zhang, Qin Liu & Mingfan Li

To cite this article: Minglei Li, Zheng Li, Meng Zhang, Qin Liu & Mingfan Li (2024) Efficient shrub modelling based on terrestrial laser scanning (TLS) point clouds, International Journal of Remote Sensing, 45:4, 1148-1169, DOI: [10.1080/01431161.2024.2305633](https://doi.org/10.1080/01431161.2024.2305633)

To link to this article: <https://doi.org/10.1080/01431161.2024.2305633>



Published online: 02 Feb 2024.



Submit your article to this journal



Article views: 97



View related articles



View Crossmark data



Citing articles: 1 View citing articles



Efficient shrub modelling based on terrestrial laser scanning (TLS) point clouds

Minglei Li^{a,b}, Zheng Li^a, Meng Zhang^c, Qin Liu^a and Mingfan Li^a

^aCollege of Electronic and Information Engineering, Nanjing University of Aeronautics and Astronautics, Nanjing, China; ^bMinistry of Education, Key Laboratory of Radar Imaging and Microwave Photonics (Nanjing University of Aeronautics and Astronautics), Nanjing, China; ^cCo-Innovation Center for Sustainable Forestry in Southern China, College of Biology and the Environment, Nanjing Forestry University, Nanjing, China

ABSTRACT

This paper presents a methodology for automatically generating 3D models of individual shrubs from point clouds acquired by Terrestrial Laser Scanning (TLS) devices. The creation of accurate 3D models for shrubs holds significant value for ecological studies. The shrub modelling is more challenging compared to other tree modelling tasks, due to the presence of substantial noise and fuzzy branch structures. To address these challenges, our approach first partitions the input point cloud into two categories: branches and others. This point segmentation process effectively eliminates interference of leaves and noise, thereby enhancing the visibility of branch skeletons. Then, we construct a triangulation network using the branch points and establish a minimum spanning tree (MST) based on this network. Serving as the initial skeleton representation of the plant, the MST preserves the essential topological structures of the branches. Within the extracted MST, we implement a recursive trimming technique to eliminate redundant branches by merging adjacent points and edges, ultimately consolidating the skeleton structure. Finally, we employ an adaptive cylinder fitting algorithm that relies on robust principal component analysis (RPCA) to generate the model. The effectiveness and robustness of the proposed method are demonstrated via experiments on different datasets, with an average fitting error of 1.13 cm, indicating that our approach can achieve high accuracy in modeling individual shrubs.

ARTICLE HISTORY

Received 19 October 2023

Accepted 10 January 2024

KEYWORDS

Shrub modelling; point cloud; point segmentation; minimum spanning tree, skeleton extraction

1. Introduction

Shrubs constitute a vital component of terrestrial ecosystems and are widely present in nature (Myers-Smith et al. 2011). Reconstructing the digital 3D models of shrubs holds substantial potential for various applications, such as ecological simulation, agricultural estimation, and forestry management (Bienert et al. 2018; Erfanifard and Khosravi 2015; Zhao et al. 2021). Shrubs modelling can help explore the mechanisms and patterns of shrub growth, providing basic data for ecosystem simulation and prediction. Detailed 3D

CONTACT Minglei Li  minglei_li@nuaa.edu.cn  College of Electronic and Information Engineering, Nanjing University of Aeronautics and Astronautics, Ministry of Education, Nanjing University of Aeronautics and Astronautics, Jiangjun Road 29, Nanjing 211106, China

© 2024 Informa UK Limited, trading as Taylor & Francis Group



models facilitate precise estimation of plant parameters such as height, width, and stem diameter, thereby enabling accurate ecological modelling and agroforestry management (Kangas and Maltamo 2006; Paturkar, Gupta, and Bailey 2021; Raumonen et al. 2015). Most shrubs contain several perennial stems that may be erected or close to the ground, such as the examples shown in Figure 1. The complex structure of shrubs makes automatically reconstructing detailed 3D models a non-trivial task.

The traditional methods for measuring shrubs are laborious and time-consuming. To compensate for extra expenses associated with the field work, terrestrial laser scanning (TLS) techniques have been successfully adopted in forest inventory (Ke and Quackenbush 2011; Liang et al. 2016; Raumonen et al. 2013). TLS devices can directly capture the 3D point clouds of the scenes and obtain accurate geometric details of objects. Individual plant detection from TLS point clouds is the basis for some inventories, including species identification in mixed forests and information gathering such as biomass, trunk volume, biodiversity, and changes in these attributes at multiple scales (Bienert et al. 2018; Maas et al. 2008). The point clouds of individual plants can be utilized to create elaborate 3D models that accurately represent their structures. While most known automated 3D modelling methods are developed for tree scans, there has been limited research specifically for shrub modelling.

To accurately construct plant models, it is essential to recover the fundamental branch shapes. There exists a set of models known as quantitative structure models (QSMs) (Raumonen et al. 2013), which represent plants as hierarchical assemblies of elemental units. These models provide data on the volumes and diameters of branch segments essential for biomass estimation. A commonly employed approach involves performing cylinder fitting on branch points, preserving the primary structural characteristics of plant shapes. Consequently, a QSM consists of a hierarchical collection of cylinders estimating topological, geometrical, and volumetric details of the woody structure of the plants.

Other geometric primitives, i.e. Pollock model (Kippers, Moth, and Oude Elberink 2021) or convex hulls (Tymkow and Borkowski 2010), also can be used to construct plant models. To reconstruct QSM models for short shrubs, the convex hull-based algorithm (Tymkow and Borkowski 2010) is used for sliced point cloud data, but the hierarchical information within the convex hull is lost. Nonetheless, there are instances where the utilization of complex primitives (i.e. with more variables and features) has yielded unstable outcomes, as these primitive fitting methods are sensitive to noise and data



Figure 1. Shrubs lack obvious main branches.

missing due to occlusions (Paturkar, Gupta, and Bailey 2021), which are common in plant scanning datasets. In general, the cylinder primitives are robust in representing the geometry of branches, although there are holes and noises in the dataset.

To enhance the accuracy of estimating the centres and radii of cylinder primitives, it is advised to maintain a uniform point density, thereby ensuring consistent data quality for 3D modelling. One possible approach involves uniformly down sampling the point cloud, such as employing voxel grid filtering (Burt et al. 2019; Wilkes et al. 2017).

Over the past decade, several methods have been developed for the purpose of segmenting individual plants from initial point clouds (Burt et al. 2019; P. Wang, Cao, and Wang 2022; Yrttimaa et al. 2019). Notice that, the primary objective of this paper is to construct comprehensive 3D models for shrubs, and therefore, the segmentation of individual plants falls beyond the scope of this paper. A feasible method to perform the segmentation of individual plants is to use software tools such as treeseg (Burt et al. 2019).

Typically, an individual shrub lacks a main branch and exhibits many leaves, which poses challenges when attempting to extract the branch skeleton. Therefore, the critical task of building a 3D model for a shrub involves recovering the topological structures of its branches from voluminous point data. It is preferred to perform branch-leaf separation as a preliminary step. Unsupervised approaches are preferred over supervised machine learning approaches considering the difficulty of acquiring manual labelling tasks (D. Wang 2020). The density features of leaves play a crucial role in branch-leaf separation (Béland et al. 2011; Liu et al. 2020; Oshio et al. 2015). To improve computational efficiency, Hui et al. (2021) proposed a separation method based on mode points evolution, transforming point-wise classification into segment-wise classification.

This paper investigates the application of TLS point cloud technology in modelling of individual shrubs growing in arid and semi-arid areas. The proposed method adopts a divide-and-conquer modelling strategy, wherein points are classified into leaves and branches according to their morphological characteristics. Furthermore, leveraging the underlying assumption of continuous growth in plant branches, a heuristic strategy is employed to precisely extract the centre of the branches. The skeletons of the branches are reconstructed by connecting adjacent meaningful segment units identified from the mass points. Ultimately, the surfaces and structures of shrubs are accurately reconstructed using the selected cylinder primitives. The main task of the proposed method is to accurately separate and model the branches of shrubs, while minimizing the interference of leaves and noises on the modelling results.

2. Related work

The trend of plant modelling from LiDAR point clouds has witnessed significant advancements and developments in recent years. However, modelling methods specifically designed for shrubs present additional challenges due to their distinct characteristics. In this section, we reviewed relevant existing modelling approaches for both trees and shrubs, categorized into segmentation-based and skeleton-based methods.

2.1. Segmentation-based methods

Segmentation-based methods aim to divide TLS point clouds into smaller subsets and subsequently connect them in a specific manner to reconstruct the topological structure of the plants. Numerous approaches have been proposed to address this problem. Su et al. (2019) used a slicing method to divide the point cloud into different subsets, and extracted the skeleton points of each subset using L1 median. Then, the skeletons of each subset were connected to obtain the complete skeleton. Ai et al. (2020) also used the method of slicing point clouds for skeleton extraction. The difference is that this method uses kernel mean shift and principal component analysis algorithms to generate the skeleton of each slice. One another commonly used method is based on clustering algorithms, such as k-means or hierarchical clustering. These techniques group points together based on their spatial proximity or other geometric properties. However, they often struggle with handling complex plants with irregular shapes and varying densities.

To effectively extract different tree components, such as trunks or individual branches, Hackenberg et al. (2015) use a hierarchical structure to represent parent-child proximity, and different cylinders are fitted on different hierarchical structures. However, this method requires manual input of key parameters such as branch radius, and requires input data to be as complete as possible with low noise, which is difficult to achieve in practice. Fu et al. (2020) introduce a cylindrical prior constraint (CPC)-based approach that employs a level set method to extract initial skeletons, followed by optimization of skeleton point positions using CPC. This method may struggle with shrubs exhibiting significant distortions. Hui et al. (2022) proposed a neighbouring growing method to over-segment the point cloud, followed by the fusion of similar segments to extract object primitives. Each object primitive was then fitted as a cylinder to construct the tree model.

Another work by Zhao et al. (2021) focuses on measuring the geometric parameters of shrubs by categorizing them into main branches, secondary branches, and fruiting branches. A software tool named CATIA is employed for constructing a 3D model based on manual measurements, resulting in rough models and limited accuracy. Yang et al. (2022) use a binocular visual system to capture the plant from multiple angles and combine the results to generate a complete 3D model. Although this method offers high reconstruction accuracy, it is time-consuming due to the need for multiple movements of the measuring equipment, and model accuracy is highly dependent on scan registration precision.

2.2. Skeleton-based methods

Different from the segmentation-based method, skeleton-based approaches directly extract skeleton curves from the input point cloud as the topological structure of the plant. There are many challenges in the automatic extraction of skeletons of branches. Achieving accurate skeletons through an algorithm is exceedingly difficult, especially when confronted with dense leaves and occlusion-induced data gaps.

While significant progress has been made in extracting skeletons from 3D point clouds in computer vision and graphics domains, handling plant structures remains an open challenge. The difficulties encountered include the zigzag nature of plant skeletons, the

non-uniform density of skeleton points, the scarcity of points in regions with complex geometry, and the lack of biological relevance.

Gaillard et al. (2021) utilize a voxel carving algorithm to generate 3D approximate skeletons of shrubs, followed by transforming the skeleton through path comparison and evaluation from each leaf to the plant root. Pruning based on biologically inspired features yields the corresponding skeleton for the input plant. This method demonstrates effectiveness in extracting skeletons of herbaceous plants like corn and sorghum but may encounter issues when dealing with shrub skeletons.

The L1 median method is widely used to extract the local centres from a point cloud. In tree modelling, several works employ the L1 median method to extract centres and connect them to generate the skeleton (Huang et al. 2013; Lu and Fan 2022; Ozbay, Cinar, and Guler 2018). However, these algorithms suffer from uneven sampling density and connectivity errors resulting from threshold-based skeleton elongation. To address these limitations, Lu and Fan (2022) propose an improved algorithm based on adaptive k-means clustering, enhancing the accuracy and repeatability of the point cloud skeleton extraction. Ozbay et al. (2018) introduce an algorithm that combines Laplace iterative shrinkage and L1-median shrinkage for skeleton extraction. By applying L1-median shrinkage to the point cloud after Laplace iterative shrinkage, these complementary methods reduce the number of iterations and exploit neighbourhood information. However, as shrub data often contain small branches and high-level noise, skeletons extracted using L1 median may exhibit positional errors and crossovers.

There are also some other different skeleton extraction methods, such as the notion of β -splines, which form a curve defined as a finite set of curves joined in a tree topology (Chaudhury and Godin 2020). Zhou and Toga (1999) proposed a voxelization coding method for 3D modelling based on distance fields. The calculation of this method is simple and insensitive to the boundary complexity, but the skeleton obtained in the discrete domain is often discontinuous. Tagliasacchi et al. (2009) proposed a method based on the rotational symmetry axis (ROSA) to extract the skeleton. For large missing multi-branch point clouds, the proposed method accurately represents the topology of the original model. However, it entails significant computational complexity.

Cao et al. (2010) introduced a skeleton extraction approach based on the Laplace operator to recover the curve. This technique incorporates local Delaunay triangulation and topology refinement on the point cloud while iteratively contracting from the outside to the inside to extract the skeleton. It demonstrates strong noise resistance and can handle point clouds with missing data. The accuracy of the skeleton relies heavily on the parameters of the Laplace operator and may result in local point cloud shrinkage.

To simulate tree growth to extract skeletons, a type of space colonization algorithm (Xu, Hu, and Xie 2022) is proposed. The method utilizes Density-Based Spatial Clustering of Applications with Noise (DBSCAN) clustering. Prior to clustering, noise filtering pre-processing is performed on the point cloud, and DBSCAN method is used to identify the number of bifurcations and enhance the visual quality of the extracted skeletons. You et al. (2020) proposed a skeleton formation method using geometric centre points to interpolate the 3D stem axis. It calculates the geometric centre point of the stem slice and then inserts the centre point into the 3D stem axis curve. In summary, while most skeleton extraction algorithms are effective for trees with prominent trunks, their efficacy for shrubs and small trees remains uncertain.



In recent years, several open-source modelling tools have emerged, such as TreeQSM (Raumonen et al. 2013), AdTree, and PypeTree (Delagrange, Christian, and Rochon 2014). TreeQSM (Raumonen et al. 2013) is a modelling tool that reconstructs QSMs for trees from point clouds. It assumes that the point cloud provides a locally uniform and sufficiently extensive sample of the tree's surface in 3D Euclidean space. AdTree (Du et al. 2019) extracts an initial tree skeleton from the input point cloud by establishing a minimum spanning tree using the Dijkstra algorithm. The method can generate good models for trees when the algorithm can extract accurate centre points and radii of different parts of branches. PypeTree (Delagrange, Christian, and Rochon 2014) is a Python-based tool with a UI for the reconstruction and modelling of botanical trees from TLS point clouds. It addresses methodological challenges associated with imperfect point cloud datasets through semi-supervised adjustment tools, producing a set of truncated cones that approximate branches.

These tools generally require point clouds with minimal noise and should not include leaf points to avoid erroneous results. Furthermore, cone-fitting methods may oversimplify structures and lead to a loss of necessary details, particularly when dealing with shrubs. This paper focuses on developing an automated and efficient modelling method for shrubs, which contain a more complex skeleton nature, non-uniform density, and geometric scarcity. We introduce a skeleton-based method that accurately constructs 3D models from individual point clouds of shrubs.

3. Methodology

Our datasets were captured using a TLS device, i.e. Leica BLK360, positioned approximately 5 metres away from the plants. Furthermore, the extraction of individual shrubs was accomplished through an effective ground filtering segmentation method based on the software treeseg (Burt et al. 2019). The original point cloud encompasses the primary branches and leaves alongside substantial noise and outliers. An overview of the proposed approach is shown in [Figure 2](#).

To enhance the quality of the data, the initial step involves performing denoising and branch-leaf segmentation. Secondly, we build a minimum spanning tree (MST) for the extraction of the initial skeleton and simplify the skeleton by merging adjacent points to handle the zigzag structures of the skeleton. The simplified skeleton undergoes a smoothing process using a Hermite interpolation refinement technique. Following this, the radii of the branch segments are determined utilizing a least square method.

Leveraging the refined skeleton segments and the estimated radii, a cylinder fitting method is employed to generate the final 3D models of the shrubs. This process facilitates obtaining accurate representations of the plant's structure and geometry.

3.1. Point segmentation

At the very beginning of the modelling, a sparse outlier removal method (Rusu and Cousins 2011) is applied to mitigate the presence of isolated individual points or clusters consisting of only a few points. The method covers the point cloud with small spheres and deletes the points in the spheres that maintain a very small number of points.

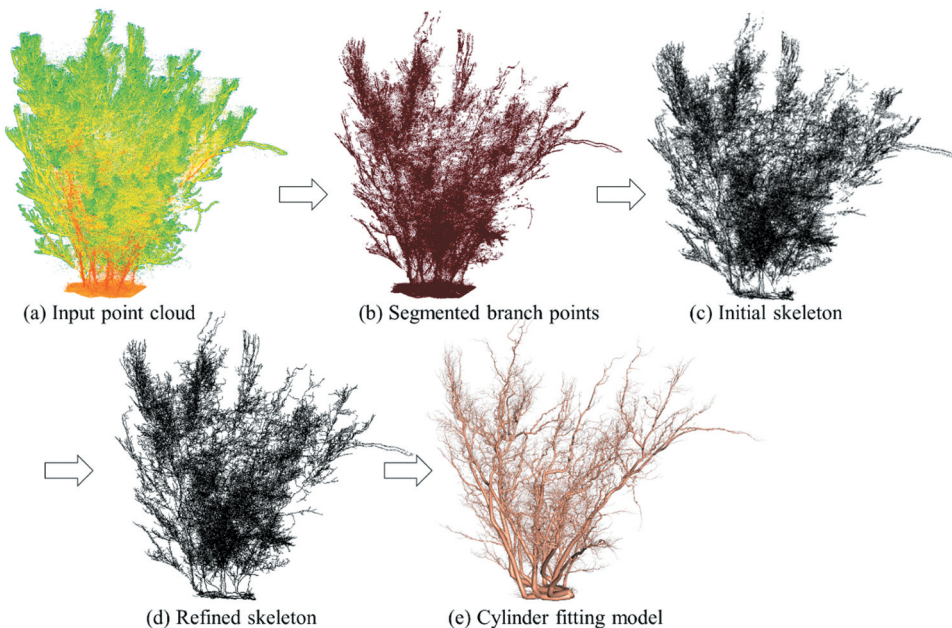


Figure 2. The pipeline of the proposed modelling method.

The branch-leaf segmentation can eliminate the influence of leaves and filter out many noises. Hence, it is useful for the consolidation of the branch skeleton and helps to accelerate the subsequent construction, as it reduces the number of points. Specifically, we introduce a novel metric that effectively characterizes the point information of branches and leaves. Subsequently, we perform segmentation based on this metric. To ensure the adaptability of our method to diverse point cloud types, we have developed a ‘soft-to-hard’ segmentation approach illustrated in Figure 3. Adaptive thresholds for density and intensity values are computed to perform the segmentation of branch points and leaf points.

The TLS devices used in our research can provide a signal intensity value for each point. These intensity values, obtained through TLS technology, represent the digital representation of echo intensity and are directly proportional to the number of photons incident on the detector. Determining the factors influencing echo intensity values is a highly intricate process, encompassing aspects such as material composition, surface roughness, incident angles, measurement distances, and object shapes (Core and Sterzai 2006; Soudarissanane et al. 2011). In the case of woody plants, the intensity values associated with branch points and leaf points tend to differ due to their distinct physical reflectivity characteristics. Branches, being rigid and stable, exhibit higher intensity values than leaves, which are flexible and variable. However, it is worth noting that intensity values of points located on small branches may resemble those of leaf points, and in some cases, the opposite scenario may even occur.

On the other hand, to estimate the density values, n points are randomly selected as seed points (representatives). Within a spherical space centred around each seed point and with a radius γ , the number of neighbouring points is tallied. This count is then

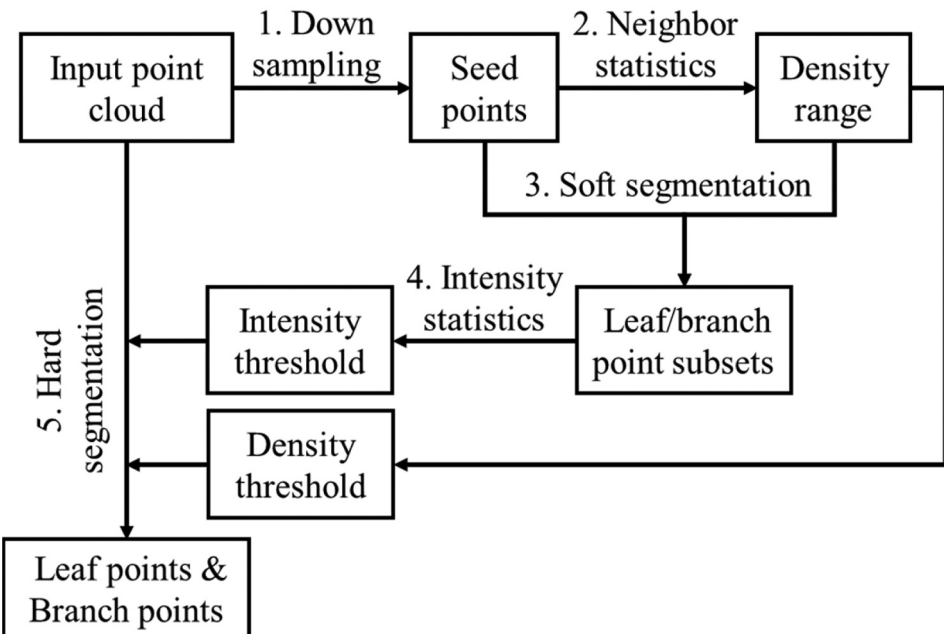


Figure 3. The “soft-to-hard” segmentation method.

considered as the density value ρ . Empirically, we set n to 1000 and γ to 0.03 metres, ensuring that the seed points adequately cover the entire regions of the plants.

After counting the density values of the seed points, a rough density range of the entire data is obtained. We divide the density range into quarters, referred to as $[\rho_{\min}, \rho_{1/4}, \rho_{1/2}, \rho_{3/4}, \rho_{\max}]$. These intervals play a crucial role in guiding the process of soft segmentation. Specifically, data points with densities exceeding $\rho_{3/4}$ are assigned to a branch point subset, while those with densities falling below $\rho_{1/4}$ are allocated to the leaf point subset. The branch and leaf subsets identified through this soft segmentation approach are subsequently utilized for intensity analysis. By constructing separate intensity histograms for the branch and leaf subsets, we can identify their intersection point, denoted as the intensity threshold represented by I_{Thr} .

A unified criterion is established to facilitate the branch-leaf segmentation. A given point is categorized as a branch point only if its density value surpasses $\rho_{1/2}$ and its intensity value is greater than I_{Thr} ; otherwise, it is identified as a leaf point. The efficacy of employing this combined criterion for branch-leaf segmentation has been successfully demonstrated. Nevertheless, during the process of eliminating leaf points, certain instances of residual noise may persist. If the noise is not completely removed, there is a concern about the effect on the reproducibility of the 3D models.

To address the issue of scattered misclassified leaf points, we employed spatial geometric information to further refine the branch points. The average distance \bar{d} between each branch point p and its K nearest neighbour points is calculated, with K empirically set to 8. A distance threshold T was then introduced to identify and

remove unreliable points from the branch point set. Points exhibiting an average distance \bar{d} smaller than T were eliminated. Following this refinement process, a revised branch point set was obtained, which served as input for the subsequent modelling procedure.

3.2. Initial skeleton extraction

To address the potential limitations arising from self-occlusions during skeleton extraction, a transformation from a point-based space to a graph-based space is employed. Graph-based methods have been utilized for point cloud analysis (Straub et al. 2022; Westling, Underwood, and Bryson 2021). These methods model the relationships between points as a graph and employ graph-based algorithms to identify regions within the point cloud. By considering both local and global connectivity information, these techniques can effectively handle intricate structures and preserve fine-grained details. By capturing both local and global contexts, graph-based skeleton extraction enhances the understanding of the overall plant structure and the branch topology present in the point cloud.

Firstly, a 3D Delaunay triangulation procedure is executed on the given point cloud, resulting in the construction of a triangulation network that serves as the input mesh for the subsequent skeleton extraction. The triangulation network could be regarded as a kind of edge-weighted graph, where the length of each triangle's edges represents its associated weight. By incorporating edges between distant points, this graph facilitates the completion of missing regions and connections among separate branches. The initial skeleton is constructed by traversing the triangulation network, and then, the nodes of the skeleton are iteratively refined by graph contraction.

The MST in this graph is defined as a spanning tree whose sum of edge weights is no larger than the weight of any other spanning tree. In this study, the MST is extracted by the Dijkstra shortest path algorithm (H. Zhou, Shenoy, and Nicholls 2002). Extracting the MST aids in identifying the most salient features and capturing the essential structure of the skeleton during the refinement process. [Figure 4](#) illustrates the initial skeleton generated through the application of the MST-based algorithm on the input points.

During calculating the MST, it is necessary to designate a root point. However, due to the distinctive shape attributes exhibited by shrubs, identifying the root directly is not apparent. Consequently, defining the starting point becomes a nontrivial task. To tackle this issue, we propose a solution by obtaining a narrow cross-section from the lower portion of the data and selecting the centre of gravity within that slice as the designated root point.

3.3. Skeleton refinement

As all branch points participate in the MST traversing, the initial skeleton exhibits a considerable number of points and edges, as shown in the enlarged part of [Figure 4](#). A compact model needs to further simplify the skeleton without compromising the accuracy of model reconstruction. This approach leverages local geometric information surrounding each point in the point cloud to refine the skeleton.

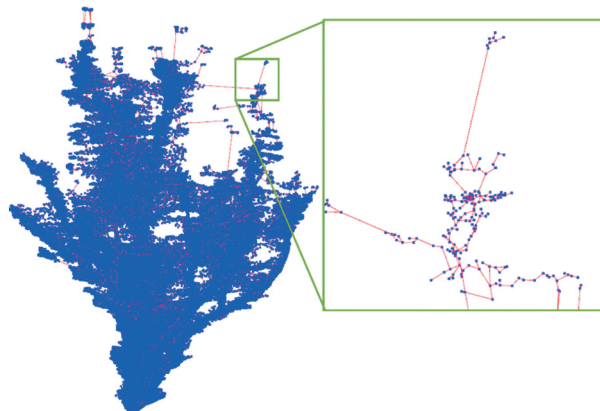


Figure 4. Initial skeleton extracted by the minimum spanning tree (MST) method.

Firstly, the initial skeleton undergoes a weight assignment process, whereby each point and edge are assigned a weight value. This enables the removal of short branches based on their weight. Subsequently, adjacent vertices are merged by detecting their proximity along the skeleton, leading to the elimination of any remaining redundant edges and points.

The weight value assigned to each point is determined by the spanning length of its corresponding sub-tree. The sub-tree of a point encompasses the point itself and all its descendant points and edges. Consequently, the weight value w_i of a given point p_i is computed as the sum of the lengths of all edges within its sub-tree.

This weighting scheme ensures that points closer to the lower region of the shrub receive higher weight values, while those nearer to the top obtain lower weight values. The root vertex is assigned the maximum weight value. An advantageous aspect of this approach is its insensitivity to the density of input points, rendering it robust to data acquired from diverse scanning qualities.

Furthermore, each edge's weight value is determined as the average of the weights of its two associated points. Consequently, the points and edges located in the upper portion of the plant consistently exhibit low weight values. On the other hand, the main branches situated near the lower region of the plant acquire larger weight values, while smaller branches adjacent to the trunk are assigned significantly smaller weight values. Such characteristics facilitate the removal of minor noisy branches present along the main branches while preserving the smaller branches in the upper area of the shrub.

After simplifying the initial skeleton by the weight value, there may still exist redundant edges and points within the structure. To address this, we employ a method that detects the proximity between adjacent points in order to further simplify these elements. A similarity score, denoted as β , is introduced to quantify the closeness between such adjacent points. Two scenarios are considered: when a point has only one child point, and when it has multiple child points.

In the process of simplifying the skeleton structure, when considering a point along with its parent and child, we observe two skeleton lines: one connecting the point to its parent, and the other connecting it to its child. The simplification involves removing the

subject point and forming a direct line segment between the parent and child points. The importance of the current point is determined by evaluating its distance to the line segment formed by its parent point and child point. If the current point is found to be closer to this line segment, its importance is diminished. Hence, a distance score β is defined as follows:

$$\beta = \begin{cases} \left(\frac{w_{\text{current}}}{w_{\max}}\right)^{1.1} \times d, & \text{if } w_{\text{current}} > \frac{w_{\max}}{4} \\ d, & \text{else} \end{cases} \quad (1)$$

where d represents the distance between the current point and a candidate line segment between the parent and child points; w_{current} is the weight of the current point, w_{\max} is the maximum weight of all points. If the distance score β is less than the given threshold σ , it is considered that the current point is less important and can be deleted from the skeleton. The formula is composed of two parts. Firstly, if a point is closer to the root, we use a scaling factor $w_{\text{current}}/w_{\max}$ multiplied by d to make the distance score β smaller. Smaller β are more likely to merge branch points, making the lower branches straighter. The use of exponential ratio 1.1 aims to fine tune the adaptability of similarity. Secondly, when the weight of the current point is less than $w_{\max}/4$, the point is typically positioned far from the root. In such scenarios, we can directly employ its distance as a measure of the distance score. This approach ensures the appropriate preservation of the details pertaining to the branches and endings. [Figure 5](#) illustrates the simplification process of deleting the current point.

In the case of points with multiple child points, we process each pair of child points individually. The distance score β follows a similar form as Equation (1), but here the distance d is calculated as follows:

$$d = \min(l_1 \sin \theta, l_2 \sin \theta) \quad (2)$$

where l_1 and l_2 represent the lengths between the current point and its two child points, and θ is the angle between the two edges of the current point and its two child points. We choose the minimum value to assess the proximity between adjacent child points. This approach allows us to obtain a set of distance scores $\{\beta_i\}$ for the current point. If the

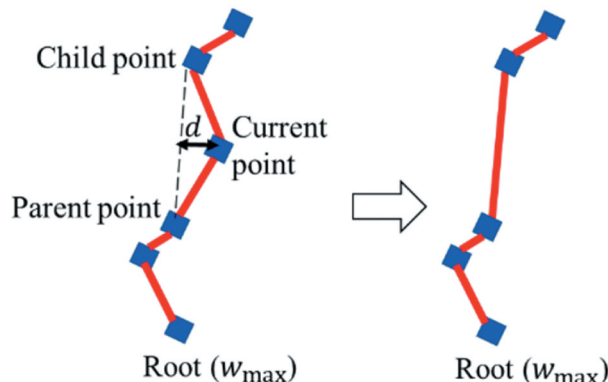


Figure 5. Points with only one child point.

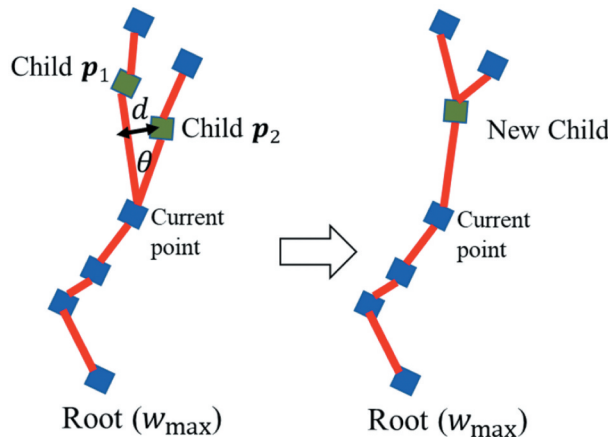


Figure 6. Skeleton simplification for points with multiple child points.

minimum similarity β_{\min} in the set, is less than the given threshold σ , then the two child points corresponding to β_{\min} need to be merged.

The merged new child point position is directly using the average of the original two child point positions. [Figure 6](#) shows the simplification process. Note that changes in the positions of points will affect the decision of whether to merge subsequent points. We adopt a simple approach by iteratively processing this merging simplification several times, which typically yields favourable results.

The similarity threshold σ plays a crucial role in controlling the level of similarity during the skeleton simplification process. We tested the value of σ from 0.5 to 2, and the corresponding results are presented in [Figure 7](#). When the simplification threshold is set too low, the degree of merging at the branch points is insufficient, which deviates from the expected characteristics of branch growth. Conversely, setting a high simplification threshold leads to excessive simplification. Based on the experimental findings, a value of 1.5 was selected as the optimal simplification threshold.

Next, the skeleton points are smoothed using Hermite interpolation. The points with multiple child points are chosen as the stable points, which remain unchanged during the Hermite interpolation. The points that have one parent and one child are considered control points. These control points will serve as anchors for the Hermite curves and should be evenly spaced along the skeleton. For each control point, estimate the tangent vectors that define the direction and magnitude of the curve at that point. Specifically, we compute the difference between adjacent points and use those differences as the tangent vectors. Next, use the control points and their corresponding tangent vectors to compute the Hermite curves. Once we have the Hermite curves, we use them to interpolate additional points between the control points, resulting in the final refined branch points.

3.4. Cylinder fitting

Using the selected branch points, we can estimate cylinder parameters that represent the branches. In practice, we use two different means to fit cylinders for the branches, which are classified into two types, i.e. trunk branches and branch tips.

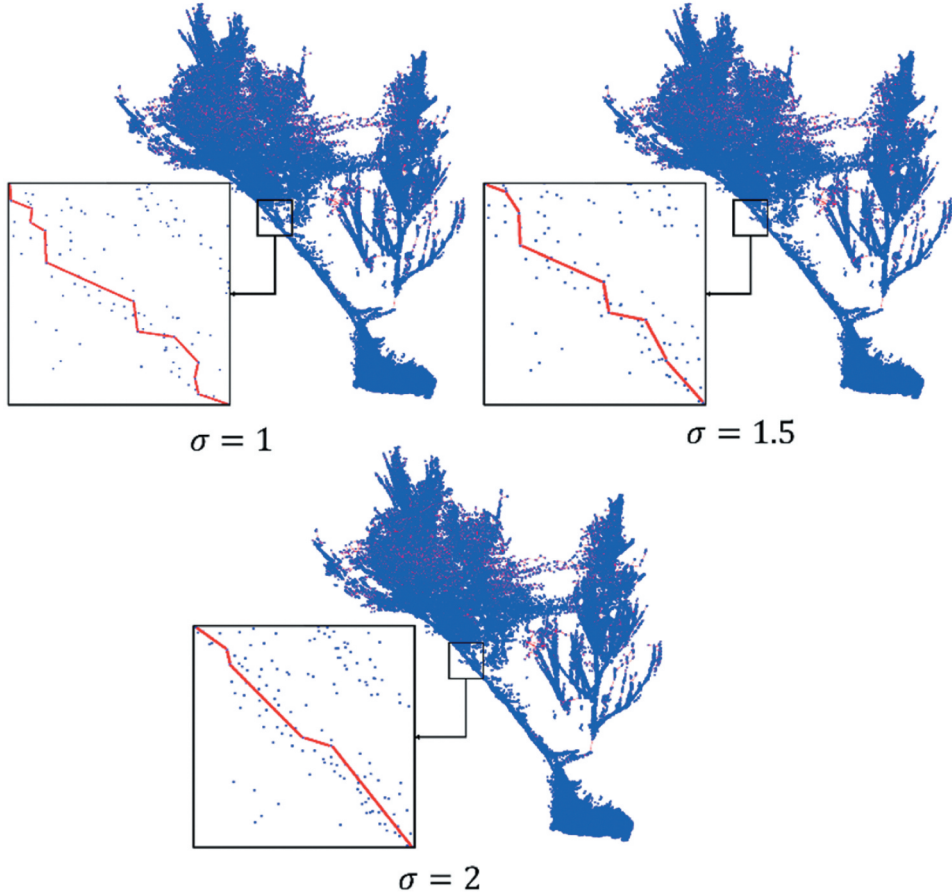


Figure 7. Simplification results using different σ thresholds.

To obtain accurate branch geometry, we employ a method based on robust principal component analysis (RPCA) (Nurunnabi et al. 2019). Firstly, we segment and identify the points near each branch. Then, we fit a cylinder surface to each branch based on the corresponding branch points to approximate the branch geometry.

The input data for the cylinder fitting is a set of branch points $\{p_i\}$. The parameters to be determined include the axial direction vector a , the position p_a of the endpoint on the axis, and the radius r of the cylinder. In this study, we employ the PCA algorithm to calculate the axial direction vector a and the position p_a . To solve radius r , we formulate an objective function that minimizes the sum of the distances from the branch points to the initial cylinder.

$$\arg \min_r \left(\sum_{i=1}^n |d_i - r| \right) \quad (3)$$

where $|d_i - r|$ represents the distance from the point p_i to the cylindrical surface; d_i is the distance between point p_i and the centreline of the cylinder. Then, the Levenberg-Marquardt (LM) algorithm (Marquardt 1963) is used to solve the nonlinear least squares problem.

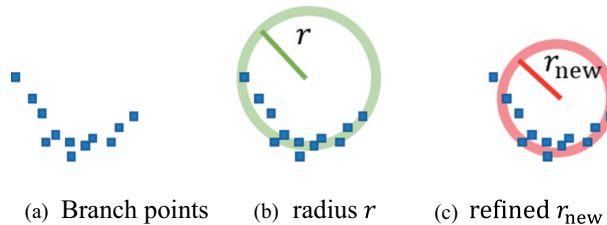


Figure 8. Using point weights to refine the radius of the cylinder.

Due to the uneven distribution of branch points, the radius r calculated by the LM algorithm may be influenced or skewed by certain noise points. To enhance the solution's quality, we use point weights to refine r . The weight λ_i of the branch point is defined as follows:

$$\lambda_i = 1 - \frac{|d_i - r|}{d_{\max}} \quad (4)$$

where d_{\max} denotes the maximum distance between all the points of the specific branch and its initial cylinder. Through formula (4), the weights of all the points of the branch are normalized. Then, the objective function is updated to:

$$\arg \min_{r_{\text{new}}} \left(\sum_{i=1}^n \lambda_i |d_i - r_{\text{new}}| \right) \quad (5)$$

Once again, we use the LM algorithm to solve formula (5) and get the adjusted r_{new} .

Figure 8 provides an illustrative example showcasing the impact of the refinement process on the radius r_{new} .

However, the points located close to the upper part of the plant tend to exhibit more noise, making it challenging to accurately perform cylindrical fitting in that region. To address this issue, we consider these branches as branch tips and calculate their radii by scaling the average radius with respect to the ratio of branch weights:

$$r_i = \bar{r} \left(\frac{w_i}{\bar{w}} \right) \quad (6)$$

where r_i represents the radius of the i -th tip branch, and \bar{r} represents the average radius of all trunk branches, which have been calculated by (5). w_i represents the weight value of the i -th branch, and \bar{w} represents the average of the weight values of all trunk branches. As described in section 'C. Skeleton Refinement', the weight value of a trunk branch is the average of the point weights of its two endpoints in the MST.

At the end, using the calculated p_a , a , and r , we can generate the cylinder surface for each branch.

4. Experiments

4.1. Experimental results

In this section, we present the analysis aimed at evaluating our modelling results. We tested a total of 13 shrubs, including three species: Haloxylon ammodendron, sand holly, and caragana. **Figure 9** presents snapshots of four representative point clouds used in this

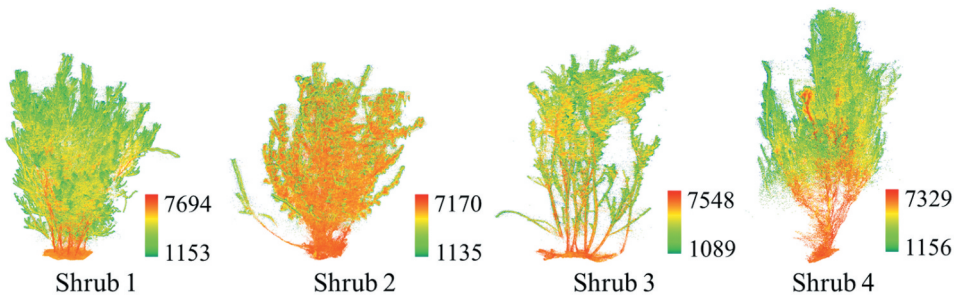


Figure 9. Snapshots of the shrub datasets with colour bars indicating the intensity values of the point clouds.

study with colour bars indicating their intensity values. Among them, shrub 1 is a *Haloxylon ammodendron*, shrub 2 is a sand holly, shrub 3 and shrub 4 are *caragana microphylla*. These shrubs grow in Gansu Province in western China and can adapt to semi-arid and desert environments. Their characteristic is that the branches are complex, and the leaves are very small.

Figure 10 presents the qualitative results obtained from the experiments. The results show that the method allows easy modelling of shrubs with different shapes and structures. It produces detailed and realistic outputs, capturing intricate shapes and proportions.

The geometrical accuracy of the modelling results is quantified by calculating the distance between the input points and the reconstructed model facets, i.e. the point to

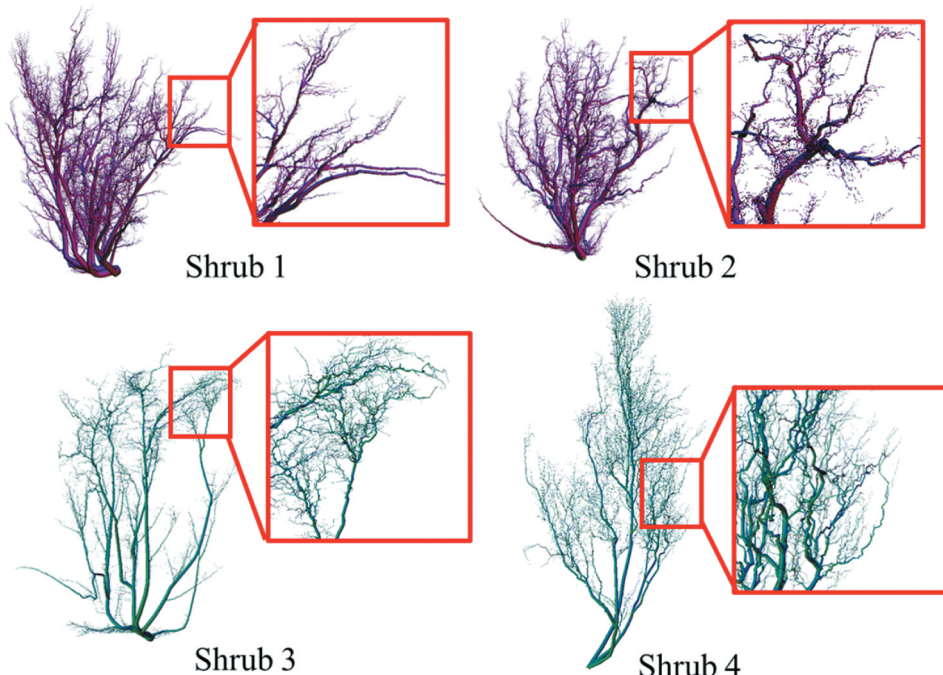


Figure 10. The visual results of the proposed algorithm.

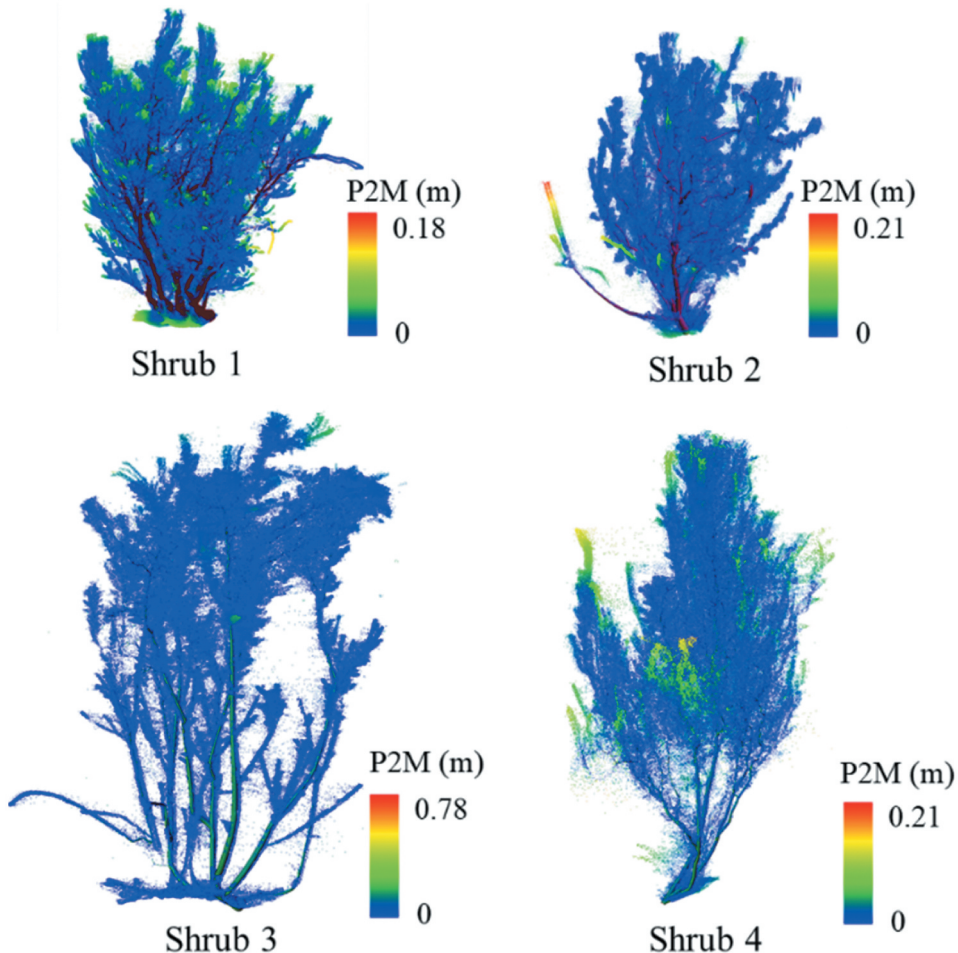


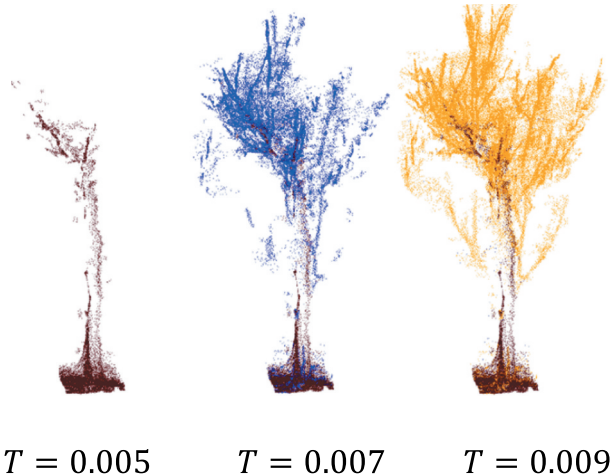
Figure 11. Point to model (P2M) distances.

model (P2M) distance. It measures how well the generated models capture the geometric features and structures of the plants. The shortest distance from each point in the original shrub point cloud to the model surface is calculated, and the original point cloud is coloured according to the distances. The closer the colour to blue, the shorter the distance. [Figure 11](#) illustrates the output quality. It is evident that most points are deep blue, indicating that the fitting errors of these points are small.

[Table 1](#) lists the average P2M distances corresponding to [Figure 11](#), which showcases an impressive average fitting error of 1.13 cm. In [Table 1](#), we use the number of main branches emerging from the roots to judge the complexity of shrubs. Compared to shrubs 2 and 4, shrubs 1 and 3 have more main branches from the roots. We observe that the points located in the main branch usually fit the models better, and the points near the tip of the branch usually have larger errors. The results demonstrate that the proposed method can generate high-precision main branch structures of shrubs. However, since the points near the tip of the branch are increasingly sparse, it is not enough to reliably reconstruct these small features from under-sampled data.

Table 1. The average point to model (P2M) distances.

Number	Point number	Complexity	Average P2M (cm)
Shrub 1	1768898	Difficult	0.94
Shrub 2	1156608	Medium	0.61
Shrub 3	1493736	Difficult	1.12
Shrub 4	725540	Medium	1.77

**Figure 12.** Segmentation results using different T thresholds.

4.2. Ablation study

In our methodology, distance threshold T is introduced in point segmentation and skeleton simplification. This section will discuss the influence of different parameter settings on the modelling results. On this basis, we select the threshold that is most suitable for our method.

The segmentation threshold T controls the segmentation degree in the point segmentation process. According to the experimental data, we test the segmentation threshold T from 0.005 to 0.009, and the results are shown in Figure 12.

We observed that the phenomenon of over-segmentation will occur when the segmentation threshold is too small, resulting in the incomplete skeleton of the final branch point. The phenomenon of under-segmentation will occur when the threshold is too large and the wrong leaf points contained in the initial branch point are not segmented. Therefore, we choose 0.007 as the segmentation threshold.

4.3. Comparisons

To further verify our solution, we quantitatively compare our method against some state-of-the-art modelling algorithms, namely TreeQSM (Raumonen et al. 2013), AdTree (Du et al. 2019), and PypeTree (Delagrange, Christian, and Rochon 2014). The modelling results are shown in Figure 13, and the average point to model (P2M) distances are measured to analyse the modelling accuracy, as listed in Table 2. In terms of the data used in the

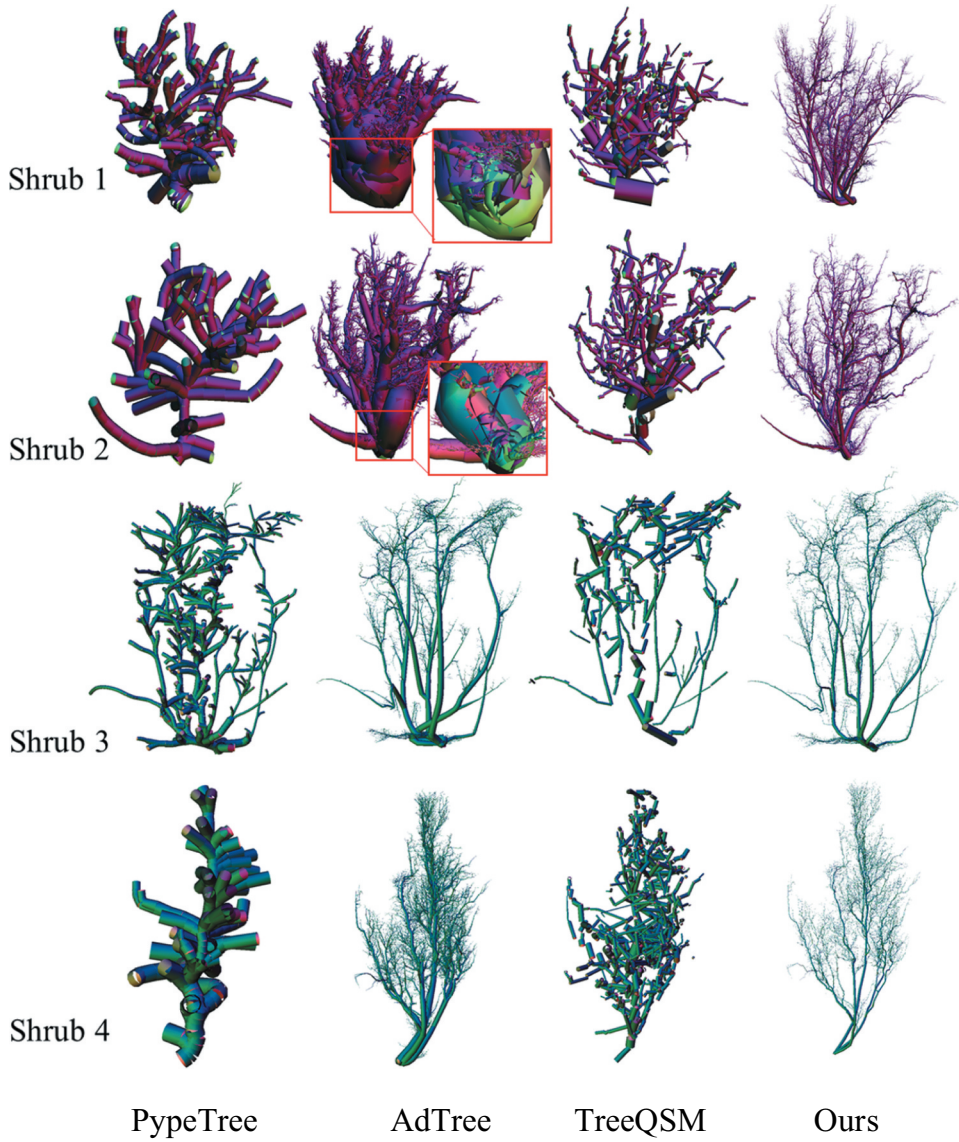


Figure 13. Modelling results of different methods.

experiment, our algorithm achieved the best accuracy. This indicates that our method has a good modelling effect on these species of shrubs growing in arid and semi-arid areas.

AdTree (Du et al. 2019) has good modelling results for trees with clear trunks. However, in this study, the models of shrubs 1 and 2 generated by AdTree (Du et al. 2019) contain a large number of redundant branches, filling the entire data space, as shown in Figure 13. Even though the P2M values of AdTree are small, the calculated distances do not correspond to the actual model facets of the points. We mark these results of shrubs 1 and 2 of AdTree as failure cases.

It can be seen from Figure 13 that the proposed method can construct models with higher topological and geometric accuracy for the test datasets. The goal of

Table 2. The average point to model (P2M) distances (cm).

	PypeTree	AdTree	TreeQSM	Ours
Shrub 1	2.35	Fail	3.10	0.94
Shrub 2	2.36	Fail	1.80	0.61
Shrub 3	2.42	1.77	3.32	1.12
Shrub 4	2.79	1.27	2.66	1.77

PypeTree (Delagrange, Christian, and Rochon 2014) is to give only a rough description of the shrub topology, and cannot restore the branch geometry. AdTree (Du et al. 2019) can extract the topological structure and branch geometry of shrubs. However, the modelling results of AdTree are very dependent on data quality. For point clouds with data missing or large amounts of noise, the modelling results are seriously distorted. And, TreeQSM (Raumonen et al. 2013) uses discrete cylinders to form a coarse 3D model, which cannot accurately obtain the actual parameters of shrubs.

5. Conclusion

This paper presents an innovative approach for the automated reconstruction of 3D models for shrubs using TLS point clouds. The method introduces a segmentation algorithm for partitioning the shrub point cloud into branch and leaf points, enabling the extraction of a distinct branch skeleton that greatly enhances the accuracy of the final shrub skeleton. Moreover, the application of cylindrical fitting based on RPCA demonstrates superior capability in capturing the geometric structure of shrub branches. Nevertheless, our approach has limitations. This method is not suitable for shrubs completely wrapped in leaves, such as urban landscape holly. In summary, our modelling method incorporates the distinctive characteristics of shrubs, and holds great potential for further advancements in understanding and exploring the intricacies of shrubs, especially for those in arid and semi-arid areas.

Disclosure statement

No potential conflict of interest was reported by the author(s).

Funding

This work was supported in part by the National Natural Science Foundation of China (42271343) and the National Natural Science Foundation of China (42177387).

ORCID

Minglei Li  <http://orcid.org/0000-0001-5432-2855>



References

- Ai, M., Y. Yao, Q. Hu, Y. Wang, and W. Wang. 2020. "An Automatic Tree Skeleton Extraction Approach Based on Multi-View Slicing Using Terrestrial LiDar Scans Data." *Remote Sensing* 12 (22): 3824. <https://doi.org/10.3390/rs12223824>.
- Béland, M., J.-L. Widlowski, R. A. Fournier, J.-F. Côté, and M. M. Verstraete. 2011. "Estimating Leaf Area Distribution in Savanna Trees from Terrestrial LiDar Measurements." *Agricultural and Forest Meteorology* 151 (9): 1252–1266. <https://doi.org/10.1016/j.agrformet.2011.05.004>.
- Bienert, A., L. Georgi, M. Kunz, H.-G. Maas, and G. von Oheimb. 2018. "Comparison and Combination of Mobile and Terrestrial Laser Scanning for Natural Forest Inventories." *Forests* 9 (7): 395. <https://doi.org/10.3390/f9070395>.
- Burt, A., M. Disney, K. Calders, and S. Goslee. 2019. "Extracting Individual Trees from Lidar Point Clouds Using TreeSeg." *Methods in Ecology and Evolution* 10 (3): 438–445. <https://doi.org/10.1111/2041-210X.13121>.
- Cao, J., A. Tagliasacchi, M. Olson, H. Zhang, and Z. Su. 2010. "Point Cloud Skeletons via Laplacian Based Contraction." In *Proceedings of the 2010 Shape Modeling International Conference*, Aix-en-Provence, France, 187–197, Provence.
- Chaudhury, A., and C. Godin. 2020. "Skeletonization of Plant Point Cloud Data Using Stochastic Optimization Framework." *Frontiers in Plant Science* 11:1–12. <https://doi.org/10.3389/fpls.2020.00773>.
- Core, F., and P. Sterzai. 2006. "Radiometric Correction in Laser Scanning." *International Journal of Remote Sensing* 27 (15): 3097–3104. <https://doi.org/10.1080/01431160500217277>.
- Delagrange, S., J. Christian, and P. Rochon. 2014. "PypeTree: A Tool for Reconstructing Tree Perennial Tissues from Point Clouds." *Sensors* 14 (3): 4271–4289. <https://doi.org/10.3390/s140304271>.
- Du, S., R. Lindenbergh, H. Ledoux, J. Stoter, and L. Nan. 2019. "AdTree: Accurate, Detailed, and Automatic Modeling of Laser-Scanned Trees." *Remote Sensing* 11 (18): 2074–2092. <https://doi.org/10.3390/rs11182074>.
- Erfanifard, Y., and E. Khosravi. 2015. "Modeling the Spatial Distribution of Sshnan (Seidlitzia Rosmarinus) Shrubs to Exploring Their Ecological Interactions in Drylands of Central Iran." *The International Archives of the Photogrammetry, Remote Sensing and Spatial Information Sciences XL-1-W5:163–168*. <https://doi.org/10.5194/isprsarchives-XL-1-W5-163-2015>.
- Fu, L., J. Liu, J. Zhou, M. Zhang, and Y. Lin. 2020. "Tree Skeletonization for Raw Point Cloud Exploiting Cylindrical Shape Prior." *Institute of Electrical and Electronics Engineers Access* 8:27327–27341. <https://doi.org/10.1109/ACCESS.2020.2971549>.
- Gaillard, M., C. Miao, J. Schnable, and B. Benes. 2021. "Sorghum Segmentation by Skeleton Extraction." In *European Conference on Computer Vision*, Glasgow, UK, 28 Aug, 2020, 296–311.
- Hackenberg, J., H. Specker, K. Calders, M. Disney, and P. Raumonen. 2015. "SimpleTree-An Efficient Open Source Tool to Build Tree Models from TLS Clouds." *Forests* 6 (11): 4245–4294. <https://doi.org/10.3390/f6114245>.
- Huang, H., S. Wu, D. Cohen-Or, M. Gong, H. Zhang, G. Li, and B. Chen. 2013. "L1-Medial Skeleton of Point Cloud." *ACM Transactions on Graphics* 32 (4): 1–10. <https://doi.org/10.1145/2461912.2461913>.
- Hui, Z., Z. Cai, B. Liu, D. Li, H. Liu, and Z. Li. 2022. "A Self-Adaptive Optimization Individual Tree Modeling Method for Terrestrial LiDar Point Clouds." *Remote Sensing* 14 (11): 2545. <https://doi.org/10.3390/rs14112545>.
- Hui, Z., S. Jin, Y. Xia, L. Wang, Y. Y. Ziggah, and P. Cheng. 2021. "Wood and Leaf Separation from Terrestrial LiDar Point Clouds Based on Mode Points Evolution." *ISPRS Journal of Photogrammetry and Remote Sensing* 178:219–239. <https://doi.org/10.1016/j.isprsjprs.2021.06.012>.
- Kangas, A. S., and M. Maltamo. 2006. *Forest Inventory: Methodology and Applications*. Berlin: Springer.
- Ke, Y., and L. J. Quackenbush. 2011. "A Review of Methods for Automatic Individual Tree-Crown Detection and Delineation from Passive Remote Sensing." *International Journal of Remote Sensing* 32 (17): 4725–4747. <https://doi.org/10.1080/01431161.2010.494184>.
- Kippers, R. G., L. Moth, and S. J. Oude Elberink. 2021. "2021 Automatic Modelling of 3D Trees Using Aerial LiDAR Point Cloud Data and Deep Learning." *The International Archives of the*

- Photogrammetry, Remote Sensing and Spatial Information Sciences* XLIII-B2:179–814. <https://doi.org/10.5194/isprs-archives-XLIII-B2-2021-179-2021>.
- Liang, X., V. Kankare, J. Hyppä, Y. Wang, A. Kukko, H. Haggrén, X. Yu, H. Kaartinen, A. Jaakkola, and F. Guan. 2016. "Terrestrial Laser Scanning in Forest Inventories." *ISPRS Journal of Photogrammetry and Remote Sensing* 115:63–77. <https://doi.org/10.1016/j.isprsjprs.2016.01.006>.
- Liu, Z., Q. Zhang, P. Wang, Z. Li, and H. Wang. 2020. "Automated Classification of Stems and Leaves of Potted Plants Based on Point Cloud Data." *Biosystems Engineering* 200:215–230. <https://doi.org/10.1016/j.biosystemeng.2020.10.006>.
- Lu, B., and X. Fan. 2022. "Research on 3D Point Cloud Skeleton Extraction Based on Improved Adaptive K-Means Clustering." *Acta Automatica Sinica* 48 (8): 1994–2006.
- Maas, H.-G., A. Bienert, S. Scheller, and E. Keane. 2008. "Automatic forest inventory parameter determination from terrestrial laser scanner data." *International Journal of Remote Sensing* 29 (5): 1579–1593. <https://doi.org/10.1080/01431160701736406>.
- Marquardt, D. W. 1963. "An Algorithm for Least-Squares Estimation of Nonlinear Parameters." *Journal of the Society for Industrial and Applied Mathematics Soc* 11 (2): 431–441. <https://doi.org/10.1137/0111030>.
- Myers-Smith, I. H., B. C. Forbes, M. Wilming, M. Hallinger, T. Lantz, D. Blok, K. D. Tape, et al. 2011. "Shrub Expansion in Tundra Ecosystems: Dynamics, Impacts and Research Priorities." *Environmental Research Letters* 6 (4): 045509. <https://doi.org/10.1088/1748-9326/6/4/045509>.
- Nurunnabi, A., Y. Sadahiro, R. Lindenbergh, and D. Belton. 2019. "Robust Cylinder Fitting in Laser Scanning Point Cloud Data." *Measurement* 138:632–651. <https://doi.org/10.1016/j.measurement.2019.01.095>.
- Oshio, H., T. Asawa, A. Hoyano, and S. Miyasaka. 2015. "Estimation of the Leaf Area Density Distribution of Individual Trees Using High-Resolution and Multi-Return Airborne LiDar Data." *Remote Sensing of Environment* 166:116–125. <https://doi.org/10.1016/j.rse.2015.05.001>.
- Ozbay, E., A. Cinar, and Z. Guler. 2018. "A Hybrid Method for Skeleton Extraction on Kinect Sensor Data: Combination of L1-Median and Laplacian Shrinking Algorithms." *Measurement* 125:535–544. <https://doi.org/10.1016/j.measurement.2018.05.029>.
- Paturkar, A., G. S. Gupta, and D. Bailey. 2021. "Making Use of 3D Models for Plant Physiognomic Analysis: A Review." *Remote Sensing* 13 (11): 2232. <https://doi.org/10.3390/rs13112232>.
- Raumonen, P., E. Casella, K. Calders, S. Murphy, M. Åkerblom, and M. Kaasalainen. 2015. "Massive-scale tree modelling from TLS data." *ISPRS Annals of the Photogrammetry, Remote Sensing & Spatial Information Sciences* II-3/W4:189–196. <https://doi.org/10.5194/isprsaannals-II-3-W4-189-2015>.
- Raumonen, P., M. Kaasalainen, M. Åkerblom, S. Kaasalainen, H. Kaartinen, M. Vastaranta, M. Holopainen, M. Disney, and P. Lewis. "Fast Automatic Precision Tree Models from Terrestrial Laser Scanner Data." *Remote Sensing*. 2013;5 (2): 491–520. <https://doi.org/10.3390/rs5020491>.
- Rusu, R. B., and S. Cousins. 2011. "3D is Here: Point Cloud Library (PCL)." In *IEEE International Conference on Robotics and Automation*, Shanghai, May.
- Soudarissanane, S., R. Lindenbergh, M. Menenti, and P. Teunissen. 2011. "Scanning Geometry: Influencing Factor on the Quality of Terrestrial Laser Scanning Points." *ISPRS Journal of Photogrammetry and Remote Sensing* 66 (4): 389–399. <https://doi.org/10.1016/j.isprsjprs.2011.01.005>.
- Straub, J., D. Reiser, N. Lüling, A. Stana, and H. W. Griepentrog. 2022. "Approach for Graph-Base Individual Branch Modelling of Meadow Orchard Trees with 3D Point Clouds." *Precision Agriculture* 23 (6): 1967–1982. <https://doi.org/10.1007/s11119-022-09964-6>.
- Su, Z., S. Li, H. Liu, and Z. He. 2019. "Tree Skeleton Extraction from Laser Scanned Points." *IEEE International Geoscience and Remote Sensing Symposium*, Yokohama, Japan, 28 July, 2019 - 02 August, 6091–6094.
- Tagliasacchi, A., H. Zhang, and D. Cohen-Or. 2009. "Curve Skeleton Extraction from Incomplete Point Cloud." *ACM Transactions on Graphics* 28 (71): 1–9. <https://doi.org/10.1145/1531326.1531377>.
- Tymkow, P., and A. Borkowski. 2010. "Vegetation Modelling Based on TLS Data for Roughness Coefficient Estimation in River Valley." *The International Archives of the Photogrammetry, Remote Sensing and Spatial Information Science* XXXVIII (8): 309–313.

- Wang, D. 2020. "Unsupervised Semantic and Instance Segmentation of Forest Point Clouds." *ISPRS Journal of Photogrammetry and Remote Sensing* 165:86–97. <https://doi.org/10.1016/j.isprsjprs.2020.04.020>.
- Wang, P., D. Cao, and C. Wang. 2022. "A Crown Guess and Selection Framework for Individual Tree Detection from ALS Point Clouds." *IEEE Journal of Selected Topics in Applied Earth Observations and Remote Sensing* 15:3533–3538. <https://doi.org/10.1109/JSTARS.2022.3171771>.
- Westling, F., J. Underwood, and M. Bryson. 2021. "Graph-Based Methods for Analyzing Orchard Tree Structure Using Noisy Point Cloud Data." *Computers and Electronics in Agriculture* 187:106270. <https://doi.org/10.1016/j.compag.2021.106270>.
- Wilkes, P., A. Lau, M. Disney, K. Calders, A. Burt, J. G. de Tanago, H. Bartholomeus, B. Brede, and M. Herold. 2017. "Data Acquisition Considerations for Terrestrial Laser Scanning of Forest Plots." *Remote Sensing of Environment* 196:140–153. <https://doi.org/10.1016/j.rse.2017.04.030>.
- Xu, Y., C. Hu, and Y. Xie. 2022. "An Improved Space Colonization Algorithm with DBSCAN Clustering for a Single Tree Skeleton Extraction." *International Journal of Remote Sensing* 43 (10): 3697–3713. <https://doi.org/10.1080/01431161.2022.2102950>.
- Yang, T., J. Ye, S. Zhou, A. Xu, and J. Yin. 2022. "3D Reconstruction Method for Tree Seedlings Based on Point Cloud Self-Registration." *Computers and Electronics in Agriculture* 200:168–176. <https://doi.org/10.1016/j.compag.2022.107210>.
- You, L., J. Guo, Y. Pang, S. Tang, X. Song, and X. Zhang. 2020. "3D Stem Model Construction with Geometry Consistency Using Terrestrial Laser Scanning Data." *International Journal of Remote Sensing* 42 (2): 714–737. <https://doi.org/10.1080/01431161.2020.1811919>.
- Yrttimaa, T., N. Saarinen, V. Kankare, X. Liang, J. Hyppä, M. Holopainen, and M. Vastaranta. 2019. "Investigating the Feasibility of Multi-Scan Terrestrial Laser Scanning to Characterize Tree Communities in Southern Boreal Forests." *Remote Sensing* 11 (12): 1423–1444. <https://doi.org/10.3390/rs11121423>.
- Zhao, J., S. Tsuchikawa, T. Ma, G. Hu, Y. Chen, Z. Wang, Q. Chen, Z. Gao, and J. Chen. 2021. "Modal Analysis and Experiment of a *Lycium Barbarum* L. Shrub for Efficient Vibration Harvesting of Fruit." *Agricultur* 11 (6): 519–532. <https://doi.org/10.3390/agriculture11060519>.
- Zhou, H., N. Shenoy, and W. Nicholls. 2002. "Efficient Minimum Spanning Tree Construction without Delaunay Triangulation." *Information Processing Letters* 81 (5): 271–276. [https://doi.org/10.1016/S0020-0190\(01\)00232-0](https://doi.org/10.1016/S0020-0190(01)00232-0).
- Zhou, Y., and A. W. Toga. 1999. "Efficient Skeletonization of Volumetric Objects." *IEEE Transactions on Visualization and Computer Graphics* 5 (3): 196–209. <https://doi.org/10.1109/2945.795212>.